# Signatures of Short-Range Many-Body Effects in the Dielectric Function of Silicon for Finite Momentum Transfer

Hans-Christian Weissker,[1,4] Jorge Serrano,[2] Simo Huotari,[2] Fabien Bruneval,[1,4] Francesco Sottile,[1,4] Giulio Monaco,[2] Michael Krisch,[2] Valerio Olevano,[3,4] and Lucia Reining[1,4]

[1]*Laboratoire des Solides Irradiés UMR 7642, CNRS-CEA/DSM, École Polytechnique, F-91128 Palaiseau, France*
[2]*European Synchrotron Radiation Facility (ESRF), Grenoble, France*
[3]*LEPES CNRS, UPR 11, F-38042 Grenoble, France*
[4]*European Theoretical Spectroscopy Facility (ETSF) France, Palaiseau, France*

(Received 23 July 2006; published 4 December 2006)

We present an investigation of the dynamic structure factor and of the dielectric function $\varepsilon_M(\mathbf{Q}, \omega)$ of the prototypical semiconductor silicon for finite momentum transfer, combining inelastic x-ray scattering experiments and *ab initio* calculations. In contrast with optical spectra, for finite momentum transfer time-dependent density-functional theory in the adiabatic local-density approximation together with lifetime broadening describes the physics of valence excitations correctly. Major structures in the spectra, governed by short-range crystal and exchange-correlation local-field effects, are strongly influenced by a mixing of transitions of positive and negative energies, in striking difference to spectra for vanishing momentum transfer. This mixing gives rise to a pronounced Fano asymmetry.

DOI: 10.1103/PhysRevLett.97.237602 PACS numbers: 77.84.Bw, 71.10.−w, 71.15.Dx, 78.70.Ck

Studies of electronic spectra such as optical absorption or electron energy loss give insight concerning the electronic structure of materials and often enable the extraction of related information, such as structural aspects. It can be very helpful to combine theory and experiment, especially when calculated spectra are precise enough to serve as a reference. Historically, a realistic theoretical description of optical absorption became possible only when the electron-hole interaction could be taken into account through semi-empirical [1] and, subsequently, *ab initio* [2,3] calculations of the dielectric function, based on the solution of the Bethe-Salpeter equation of many-body perturbation theory [3]. By contrast, plasmon structures in the dynamic structure factor $S(\mathbf{Q}, \omega) \propto -\mathrm{Im}1/\varepsilon_M(\mathbf{Q}, \omega)$ for vanishing momentum transfer $\mathbf{Q} \to 0$ are already reasonably well reproduced by the much less cumbersome calculations based on time-dependent density-functional theory (TDDFT) [4] in adiabatic local-density approximation (TDLDA) [5]. This has been explained [3] by the fact that the long-range contribution missing in the exchange-correlation (XC) kernel of the TDLDA is less important in the loss function $-\mathrm{Im}1/\varepsilon_M(\mathbf{Q}, \omega)$ than in the absorption spectrum.

Successful TDLDA calculations of $S(\mathbf{Q}, \omega)$ have been reported also for finite momentum transfer $\mathbf{Q}$ [6–11]. However, to our knowledge, no systematic comparison between theory and experiment existed up to now for $\varepsilon_M(\mathbf{Q}, \omega)$ at finite $\mathbf{Q}$. We have, therefore, performed an inelastic x-ray scattering experiment on silicon at beam line ID16 of the European Synchrotron Radiation Facility. Previous measurements [12] and calculations [10,12] of $S(\mathbf{Q}, \omega)$ of silicon had explained the main features. However, discrepancies seemed to indicate the need for more sophisticated many-body calculations. We show that this is not the case: The agreement between experiment and our TDLDA results turns out to be excellent even for the up to now unexplored $\varepsilon_M(\mathbf{Q}, \omega)$ that we obtain from the measured $S(\mathbf{Q}, \omega)$ by means of the Kramers-Kronig (KK) relations. This demonstrates that TDLDA contains the short-range many-body effects that are crucial for a correct description of $\varepsilon_M(\mathbf{Q}, \omega)$ in silicon.

Calculations were carried out using TDDFT on several levels of approximation. We obtain the linear-response polarizability $\chi$, and hence $\varepsilon^{-1} = 1 + v\chi$, from a Dyson-like screening equation [5]

$$\chi = \chi_0 + \chi_0(v + f_{\mathrm{xc}})\chi, \tag{1}$$

where $\chi_0$ is the independent-particle polarizability, $v$ the bare Coulomb interaction, and $f_{\mathrm{xc}}$ the functional derivative of the Kohn-Sham XC potential $v_{\mathrm{xc}}$. All quantities are functions of frequency $\omega$ and vector $\mathbf{q}$ in the Brillouin zone, and they are matrices in the reciprocal lattice vectors $\mathbf{G}$. We introduce $\varepsilon_M(\mathbf{q} + \mathbf{G}, \omega) = 1/\varepsilon^{-1}(\mathbf{q}, \omega)_{\mathbf{G},\mathbf{G}}$. Crystal local-field effects arise from the off-diagonal elements in the inversion. Without them, the matrix [13] is diagonal and $\varepsilon_M(\mathbf{Q}, \omega) = \varepsilon(\mathbf{q}, \omega)_{\mathbf{G},\mathbf{G}}$ with momentum transfer $\mathbf{Q} = \mathbf{q} + \mathbf{G}$. We use the following approximations: (i) random-phase approximation (RPA), in which $\chi_0$ is constructed with the Kohn-Sham band structure and wave functions, and $f_{\mathrm{xc}} = 0$; (ii) *GW*-RPA: same approach but with the band structure corrected for self-energy effects within the *GW* approximation [14]; (iii) TDLDA: $\chi_0$ as in (i), but the static $f_{\mathrm{xc}}(\mathbf{r}, \mathbf{r}') = \delta(\mathbf{r} - \mathbf{r}')[dv_{\mathrm{xc}}^{\mathrm{LDA}}(\rho(\mathbf{r}))/d\rho(\mathbf{r})]$; (iv) long-range contribution approximation (LRC) [15–17]: $\chi_0$ as in (ii), but $f_{\mathrm{xc}}(\mathbf{q}, \mathbf{G} = \mathbf{G}' = \mathbf{0}, \omega) = -(\alpha + \beta\omega^2)/q^2$. This simulates an $f_{\mathrm{xc}}$ derived from many-body perturbation theory [17] as an approximation. We use the parameters $\alpha$ and $\beta$ determined [16] for silicon at vanishing momentum transfer.

 

In addition, we introduce an energy-dependent lifetime broadening, following Rahman and Vignale [18]. The respective imaginary energies, taken from a fit of the modulus of the imaginary part of the self-energy matrix elements of Ref. [19], have been added in the energy denominator of $\chi_0$. We assume hence that (i) TDLDA does essentially not describe lifetime broadening, and (ii) the main effect beyond TDLDA stems from the finite lifetimes of the electrons and the holes, without lifetime corrections from the electron-hole interaction.

The ground-state and *GW* calculations are done with the plane-wave pseudopotential code ABINIT [20]. Employing the DP code [21], $\chi_0$ is constructed using Kohn-Sham wave functions and energies calculated at a regular grid of 2048 off-symmetry [22] **k** points. Subsequently, Eq. (1) is solved. Depending on the energy range, between 70 and 200 bands, 89 and 259 **G** vectors for the wave functions, and between 51 and 89 for the matrix have been used. The *GW* energy corrections have been calculated for 10 **k** points and then interpolated. All curves have been convoluted with a Gaussian of 1.1 eV full width at half maximum (FWHM).

Nonresonant inelastic x-ray scattering measurements of $S(\mathbf{Q}, \omega) = -(\hbar Q^2)/(4\pi^2 e^2 n)\mathrm{Im}1/\varepsilon_M(\mathbf{Q}, \omega)$, $n$ being the electron density, were performed for **Q** between 0.27 and 2.4 a.u. along the [100] and [111] directions at room temperature using monochromatic x rays of 7.909 keV. A silicon wafer of 1 $\mathrm{cm}^2$ surface and 65 $\mu$m thickness oriented with the normal along the [110] direction was employed in Laue geometry. Most of the spectra were taken using an energy resolution of 1.1 eV FWHM and a momentum-transfer resolution better than 0.15 a.u. No additional spectral features were observed upon increase of the energy resolution to 0.2 eV. The background was subtracted by estimating it from the signal measured for negative energy loss. The spectra were first normalized to the incoming photon flux. The elastic line was subsequently subtracted by using an exponential fit to its high-energy tail. This procedure yields reliable spectra above $\sim$3 eV. Because of the presence of the $L$ absorption edge at 99.8 eV, the spectra were extrapolated from 98 eV up to 200 eV with an exponential tail. The sum rule $\int_0^\infty S(\mathbf{Q}, \omega)\omega d\omega = Q^2/2$ (atomic units) was then applied to obtain the dynamic structure factor $S(\mathbf{Q}, \omega)$ on an absolute scale [7]. Only results for [111] are presented here, without loss of generality.

The Kramers-Kronig analysis is carried out on the normalized spectra after a suitable extrapolation to $\omega \to 0$. The KK analysis is extremely sensitive to the normalization for the smaller momentum transfers. For that reason we calculate, for both the experimental and the TDLDA results, the normalization integral $\int_0^\omega d\omega' \omega' S(\mathbf{Q}, \omega')$ which for $\omega \to \infty$ yields the sum rule that should also be satisfied in TDLDA [23]. Along with the extreme similarity of the experimental and the TDLDA results, this allows us to assume that at the high-energy tail the value of the integrals should be the same. We take the largest and the smallest ratio of the two within the considered range as maximal correction factors to the normalization. This defines the error bar for $\varepsilon_M(\mathbf{Q}, \omega)$.

We show in Fig. 1 the measured dynamic structure factor $S(\mathbf{Q}, \omega)$ along with our TDLDA and RPA calculations and an older measurement [12,24]. Thanks to the better resolution, structures such as the shoulder at about 16 eV in Fig. 1(a) can now clearly be detected. TDLDA is consistently better than RPA. The TDLDA result in Fig. 1(b) obtained using an energy-independent broadening (of 0.1 eV) shows correctly the sharp feature at about 18 eV but greatly overestimates the high-energy structures similar to those in Ehrnsperger and Bross [10]. Our approximate inclusion of the lifetimes leaves the sharply structured low-energy side intact while reducing the deviations, thus providing evidence that these structures are physical but smoothed out by lifetime effects. The excellent agreement of the TDLDA calculations with experiment, including subtle features at low energy, is striking but consistent with other encouraging results, in particular, for excitations of $s$ and $p$ valence electrons [6–11].

Much less is known concerning the capability of TDLDA to reproduce the experimental $\varepsilon_M(\mathbf{Q}, \omega)$. In Fig. 2, we compare the TDLDA result with the experimental $\varepsilon_M(\mathbf{Q}, \omega)$ obtained using the KK relations. As in the

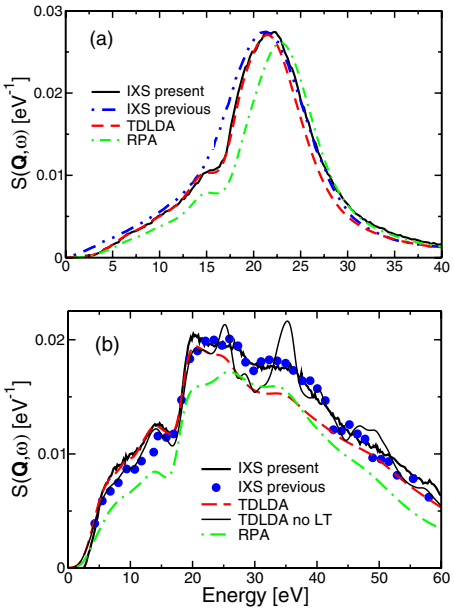


FIG. 1 (color online). (a) Dynamic structure factor $S(\mathbf{Q}, \omega)$ measured at $Q = 0.80$ a.u. along [111]. Black solid line—present experiment; blue dotted-dotted-dashed line—experiment of Schülke *et al.* [12]. The latter has been slightly rescaled in order to have the same peak height as the present experiment. Red dashed line—TDLDA; green dotted-dashed line—RPA. (b) Same as (a) for $Q = 1.45$ a.u. along [111]. The experiment (blue circles) is from Sturm *et al.* [24]. In addition, a TDLDA calculation without lifetime broadening is included as a thin solid black line.

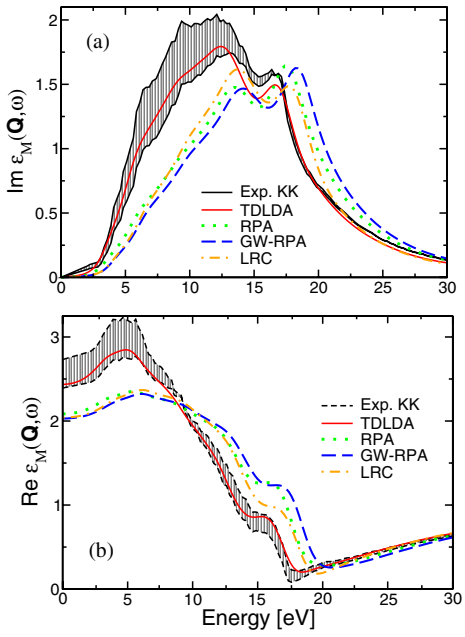


FIG. 2 (color online). Dielectric function $\varepsilon_M(\mathbf{Q}, \omega)$ for $\mathbf{Q} = 0.80$ a.u. along [111]. (a) Im$\varepsilon_M(\mathbf{Q}, \omega)$. Shown are the result of the Kramers-Kronig transformation of the experimental $\varepsilon_M(\mathbf{Q}, \omega)$ with the error bar from the normalization procedure (shaded area), TDLDA (red solid line), RPA (green dotted line), *GW*-RPA (blue dashed line), and LRC (orange dotted-dashed line). (b) Same as (a) for Re$\varepsilon_M(\mathbf{Q}, \omega)$.

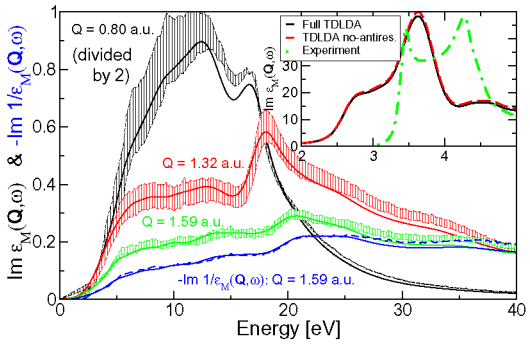


FIG. 3 (color online). Im$\varepsilon_M(\mathbf{Q}, \omega)$ for $\mathbf{Q} = 0.80$, 1.32, and 1.59 a.u. as indicated, all along [111]. Shown is the TDLDA (solid line) and the result of the Kramers-Kronig transformation of the experimental $S(\mathbf{Q}, \omega)$ [dashed line, shaded as in Fig. 2(a)]. For the largest $\mathbf{Q}$, the TDLDA (blue solid line) and the measured (blue dashed line) loss function $-\text{Im}1/\varepsilon_M(\mathbf{Q}, \omega)$ has been shown as well. Inset: Situation for $\mathbf{Q} = 0$: TDLDA (black solid line) and TDLDA without antiresonant contributions (red dashed line) are almost indistinguishable but far from experiment (green dotted-dashed line) [31].

case of the structure factor, the agreement is excellent. This success is indeed due to exchange-correlation effects in TDLDA and not just to the classical Hartree contribution; the result of the RPA, and even more of the *GW*-RPA, stands in much poorer agreement with experiment. Since the difference between *GW*-RPA and experiment is mainly due to the electron-hole interaction, we conclude that TDLDA reproduces significant excitonic effects for finite momentum transfer. These effects are only implicitly contained in TDLDA: The full TDDFT kernel contains a contribution that simulates the quasiparticle gap correction and a second term responsible for the electron-hole interaction [25,26]. The two contributions cancel partially, and TDLDA merely has to reproduce the remaining correction. Our results demonstrate that the latter should have a significant short-range contribution that is well described by a local approximation. Figure 2 shows also the result using the LRC kernel. It corrects the *GW*-RPA but by far not enough; a weak long-range contribution alone is now not sufficient to explain the spectra. LRC performs better for the plasmon peak (not shown here) but still slightly less well than TDLDA. These findings are systematic and apply to Re$\varepsilon_M(\mathbf{Q}, \omega)$ as well; cf. Fig. 2(b).

Figure 3 shows the evolution of Im$\varepsilon_M(\mathbf{Q}, \omega)$ with increasing $\mathbf{Q}$. One can follow the shift of oscillator strength towards higher energy, the formation of a peak at about 17 eV for intermediate $\mathbf{Q}$, and of a broad continuum for larger $\mathbf{Q}$. TDLDA performs very well for all investigated values of $\mathbf{Q}$, unlike for $\mathbf{Q} \to 0$ where it fails to improve upon the RPA [3,27]. For the highest momentum transfer, we also show the experimental loss function. For increasing $\mathbf{Q}$, short-range effects dominate and the screening that causes the difference between Im$\varepsilon_M(\mathbf{Q}, \omega)$ and $-\text{Im}1/\varepsilon_M(\mathbf{Q}, \omega)$ [3,28] becomes less and less relevant until they become equal.

Contrary to what one would expect, the interpretation of Im$\varepsilon_M(\mathbf{Q}, \omega)$ in terms of band structure is not straightforward. As shown in Fig. 4 (inset), an RPA calculation neglecting crystal local-field effects does not display the peak between 15 and 20 eV. The full RPA calculation, by contrast, strongly shifts oscillator strength to higher energies and in this way creates this feature (which is then simply improved by going to TDLDA). This demonstrates that crystal local-field effects become very important on the high-energy side of the spectrum, much beyond their impact in the optical spectra and similarly to findings for $-\text{Im}1/\varepsilon_M(\mathbf{Q}, \omega)$ as, for instance, in Ref. [8]. Because of the matrix inversion that yields $\varepsilon_M(\mathbf{Q}, \omega)$, the local-field effects mix transitions of different energy. For optical spectra, this mixing involves a moderate energy range. At vanishing momentum transfer, one can therefore usually neglect transitions of negative energy (antiresonant contribution) in the calculation of Im$\varepsilon(\omega)$ (see inset in Fig. 3). This fact is exploited especially for the cumbersome Bethe-Salpeter calculations [29]. An increasing though moderate importance of the coupling of resonant and antiresonant contributions with increasing $\mathbf{Q}$ has been found for the *static* structure factor of *jellium* by Tsolakidis, Shirley, and Martin [30]. Our results show drastic consequences of the antiresonant contributions for *frequency-dependent* spectra of *real* materials: Local-field effects create a sharp peak at about 27 eV (inset in Fig. 4) when only resonant contributions are considered. Inclusion of the

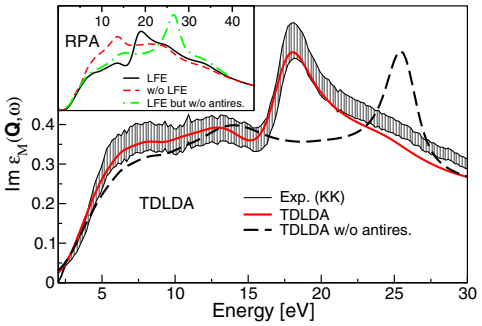


FIG. 4 (color online). Effect of antiresonant contribution on $\mathrm{Im}\varepsilon_M(\mathbf{Q}, \omega)$ for $\mathbf{Q} = 1.32$ a.u. along [111]. Shown are the result of the KK (shaded), the TDLDA (solid red line), and the TDLDA calculated without the antiresonant part (black dashed line). The inset shows RPA calculations at the same $\mathbf{Q}$, viz., RPA with crystal local fields included (black solid line), RPA neglecting crystal local fields (red dashed line), and RPA without antiresonant contributions (green dotted-dashed line).

antiresonant part makes it appear at about 19 eV. Moreover, it induces a pronounced Fano asymmetry: The sharp peak couples to the screening background of transitions of negative energy. A Fano profile has also been observed in the plasmon spectrum, in earlier measurements [12,24] and here; cf. Fig. 1(b). A model calculation suggested [12,24] that it originated from local-field effects, which is confirmed and further elucidated here. Comparison of the full TDLDA calculation to experiment demonstrates that such a parameter-free *ab initio* calculation perfectly captures the phenomenon.

In conclusion, our combined experimental and theoretical investigation provides new insight into the electronic spectra of bulk silicon. In particular, we studied $\varepsilon_M(\mathbf{Q} \neq 0, \omega)$. For finite momentum transfer, TDLDA complemented by lifetime effects performs much better than previously thought and is the method of choice for this kind of system. It reproduces continuum exciton effects, being a reliable tool for calculations of both the dynamical structure factor and, more surprisingly, the dielectric function at finite $\mathbf{Q}$.

For larger momentum transfers, short-range effects dominate the spectra; in particular, crystal local-field effects become crucial for the description of the high-energy side of the spectra, and the coupling between resonant and antiresonant contributions is of paramount importance for the correct description of the major structures: It determines the position of the main peak and gives rise to a strong Fano asymmetry. These spectra can therefore not be interpreted simply on the basis of the band structure only, and it is crucial to combine theory with experiment in order to understand the origin of the measured structures.

Fruitful discussions with A. Kaprolat, R. M. Martin, R. Del Sole, F. Bechstedt, and Gy. Vankó are gratefully acknowledged. The work was supported by the European Union through the NANOQUANTA Network of Excellence No. NMP4-CT-2004-500198 and the Marie Curie Training Site No. HPMT-CT-2001-00368. Beam time was provided by the European Synchrotron Radiation Facility. Computer time was granted by IDRIS Project No. 020544 on the NEC SX5. H.-Ch. W. acknowledges support from the European Union through the Marie Curie Fellowship No. MEIF-CT-2005-025067.

[1] W. Hanke and L. J. Sham, Phys. Rev. Lett. **43**, 387 (1979).
[2] G. Onida *et al.*, Phys. Rev. Lett. **75**, 818 (1995).
[3] G. Onida, L. Reining, and A. Rubio, Rev. Mod. Phys. **74**, 601 (2002), and references therein.
[4] E. Runge and E. K. U. Gross, Phys. Rev. Lett. **52**, 997 (1984).
[5] E. K. U. Gross and W. Kohn, Phys. Rev. Lett. **55**, 2850 (1985).
[6] N. Maddocks, R. Godby, and R. Needs, Europhys. Lett. **27**, 681 (1994).
[7] J. Tischler *et al.*, Phys. Status Solidi B **237**, 280 (2003).
[8] I. Gurtubay *et al.*, Phys. Rev. B **72**, 125117 (2005).
[9] A. G. Marinopoulos *et al.*, Phys. Rev. Lett. **89**, 076402 (2002).
[10] M. Ehrnsperger and H. Bross, J. Phys. Condens. Matter **9**, 1225 (1997).
[11] S. Waidmann *et al.*, Phys. Rev. B **61**, 10 149 (2000).
[12] W. Schülke *et al.*, Phys. Rev. B **52**, 11 721 (1995).
[13] Note that one has to be careful with the interpretation of this quantity: Whereas for cubic systems at vanishing momentum transfer longitudinal and transverse response coincide, this is no longer true for larger $\mathbf{Q}$: We are dealing with longitudinal quantities here.
[14] L. Hedin, Phys. Rev. **139**, A796 (1965).
[15] S. Botti *et al.*, Phys. Rev. B **69**, 155112 (2004).
[16] S. Botti *et al.*, Phys. Rev. B **72**, 125203 (2005).
[17] L. Reining *et al.*, Phys. Rev. Lett. **88**, 066404 (2002).
[18] S. Rahman and G. Vignale, Phys. Rev. B **30**, 6951 (1984).
[19] A. Fleszar and W. Hanke, Phys. Rev. B **56**, 10 228 (1997).
[20] http://www.abinit.org.
[21] V. Olevano *et al.*, http://theory.polytechnique.fr/codes/dp.
[22] L. X. Benedict, E. L. Shirley, and R. B. Bohn, Phys. Rev. B **57**, R9385 (1998).
[23] We use TDLDA without lifetime broadening.
[24] K. Sturm, W. Schülke, and J. R. Schmitz, Phys. Rev. Lett. **68**, 228 (1992).
[25] F. Bruneval *et al.*, Phys. Rev. Lett. **94**, 186402 (2005).
[26] R. Stubner, I. V. Tokatly, and O. Pankratov, Phys. Rev. B **70**, 245119 (2004).
[27] V. I. Gavrilenko and F. Bechstedt, Phys. Rev. B **54**, 13 416 (1996).
[28] F. Sottile *et al.*, Int. J. Quantum Chem. **102**, 684 (2005).
[29] S. Albrecht *et al.*, Phys. Rev. Lett. **80**, 4510 (1998).
[30] A. Tsolakidis, E. L. Shirley, and R. M. Martin, Phys. Rev. B **69**, 035104 (2004).
[31] P. Lautenschlager *et al.*, Phys. Rev. B **36**, 4821 (1987).